Computational Modelling of poly(9-vinylcarbazole)/Fullerene nanoheterojunction for organic solar cells and photovoltaics applications – A DFT Approach

V. W. Elloh[a,b,e,*], K. Kan-Dapaah[d], G. H. Gebreyesus[c], E. Okoampa Boadu[e], I. Arhin[e], D. F. Ofosuhene[e], D. Abbeyquaye[e], D. E. Anderson[e], D. Dodoo-Arhin[b], K. M. Abhishek [a], Eric K. K. Abavare[f], A. Yaya[b].

[a]Department of Physics, University of Petroleum and Energy Studies (UPES), Dehradun, India.

[b]Department of Materials Science and Engineering, University of Ghana, Legon, Ghana.

[c]Department of Physics, University of Ghana, Legon, Ghana.

[d]Department of Biomedical Engineering, University of Ghana, Legon, Ghana.

[e]Department of Biomedical Engineering, Koforidua Technical University, Koforidua, Ghana.

[f]Department of Physics, KNUST, Kumasi, Ghana.

*Corresponding Author's Email: vanw.elloh@ktu.edu.gh

Abstract

Organic polymer photovoltaics have a great technological potential as an alternative source for electrical energy. The demand for inexpensive, renewable energy sources is the driving force for new approaches in the production of low-cost polymer solar cells. During the quest to determine the best deposition and thermal annealing procedures of organic materials in organic devices, it has become increasingly clear that the structural order of these materials is a key factor. Highly ordered aggregation of conjugated oligomers and polymers can improve properties such as charge transfer and interaction with light processes that lead to better devices performance. The development of such procedures for polymers and their blends although successful, has taken on a substantial try and error approach. Structural and morphological characterization of organic materials in the solid state is relevant for their application in Organic Photovoltaics. A comprehensive investigation of PVK/C_{60} adsorption surface is performed using ab-initio density functional theory calculations combined with van der Waals corrections (GGA+vdW). The goal is to use detailed atomistic computational approaches to model intrinsic electrical and optical properties, to investigate the influence of packing arrangements on the anisotropy of properties which relate to device performance, to elucidate the behaviour of active materials during deposition and thermal treatment impacts on resulting morphologies which are relevant to the development of devices.

Key words: DFT; GGA-PBE; LDA-PZ; Optoelectronics; PVK; Nanoheterojunction; Organic photovoltaic.

1. Introduction

The rise of organic electronics and photovoltaics stands as one of the possible answers to appease the demand for a sustainable and risk-free future of electronics and solar energy industries. However, the implications of the development of organic electronics and photovoltaics, do not

stop at answering environmental concerns but also open up the possibility of new technological advances. Electronic devices with organic materials as active components, such as organic field-effect transistors (OFETs), organic light-emitting diodes (OLEDs) and organic solar cells (OSCs), have transitioned from scientific curiosities to potentially important technologies for consumer electronics and renewable energy converted from sun light.

Extensive research in fullerene chemistry has led to developments in photovoltaics and light-harvesting devices which may eventually lead to new efficient organic solar cells [**1**]. Research in carbon nanomaterials chemistry has provided major advancements in the use of these nanostructures in diverse areas including composite materials, electronics, drug-delivery systems, and in nanosized biosensors [**2**]. "The main interest in fullerene C_{60} stems from its unique three-dimensional structure [**3**] and remarkable electronic properties which make it useful for a range of applications in different fields including artificial photosynthesis and light-harvesting devices, electronics, energy storage, superconductors and in tribology [**4**]. Due to its properties, fullerene C_{60} is particularly useful as electron acceptor component in donor-acceptor systems for artificial photosynthesis and light harvesting devices since the electron accepting properties of fullerene C_{60} was first experimentally demonstrated in 1990 [**5**].

Fullerene C_{60} has a high electron affinity and can accept up to six electrons in a reversible manner. This electron accepting property is due to a low lying triply degenerate lowest unoccupied molecular orbital (LUMO) which is around 1.8 eV above its five-fold degenerate highest occupied molecular orbital (HOMO) [**6**]. Fullerene C_{60} is capable of carrying charges, as these can be efficiently stabilized by conjugation in the molecule [**7**]. Another important property that makes fullerene C_{60} suitable for applications in light harvesting devices is its low reorganizational energy which results from its rigid three-dimensional structure [**3**]. This facilitates fast, efficient electron transfer to occur in donor-acceptor systems [**6**].

OSCs are based on the junction of a donor and an acceptor material. The junction can be achieved simply by depositing the two materials in two separate layers [**8**], which can be controlled quite nicely, however, the architecture of choice is that of the bulk-heterojunction (BHJ) solar cell. In this architecture, donor (D) and acceptor (A) materials are finely dispersed in the active layer maximizing the D-A interface area. The photovoltaic effect in the active layer is based on the diffusion of an exciton at the donor/acceptor interface by a precise sequence of events: excitation of the D upon absorption of light; energy transfer from D to A through dissociation of the exciton and formation of a positive charge (hole) on D and a negative charge on A; migration and collection of electrons at the cathode and holes at the anode.

Recently, the design and synthesis of high-performance nonlinear optical materials has attracted significant attention for the reason that they possess huge potentials of applicability in structural engineering, optoelectronics and biomechanics [**9-12**]. For all known nonlinear optical materials, fullerenes (C_{60}) have gained tremendous interests of researchers due to their fascinating nonlinear optical properties [**13-16**]. Their high nonlinearity in optical response is mainly due to their conjugated π-electrons. The nonlinearity in optical response properties of fullerenes (C_{60}) can be significantly enhanced through functionalization with polymers. The incorporation of C_{60} into conductive polymers with variable stacking patterns and dimensions produce miniaturized

electronic and optical systems with high efficient performance in optoelectronic devices [**17**-**19**]. This augmentation in electron carrier mobility of C_{60}/polymer nanocomposite is due to the intrinsic transport characteristics of the C_{60}. A coherent perspective for incorporating C_{60} into practical devices is by way of non-covalent binding of C_{60}/polymer nanocomposites [**20**-**25**].

Polymers possessing strong affinity to undergo physical adsorption on C_{60} are promising adsorbents in facilitating amplification of interfacial binding between a polymer matrix and C_{60}. The extent of interfacial binding in this circumstance entirely relies heavily on the geometrical conformation of the polymer with respect to the C_{60}. The charge transfer processes would be governed by the electronic structure of donor-acceptor interfaces as well as the electron-phonon coupling" [**26**-**36**]. In this work, we perform density functional theory calculations combined with van der Waals corrections (GGA+vdW) to investigate the effects of different orientations of stacking structures of PVK/C_{60} nanoheterojunction on its structural and electronic properties, optical absorption spectra and charge transfer processes.

2. Computational Methodology

All the calculations are performed in the framework of density functional theory (DFT) using the QUANTUM ESPRESSO" code version 6.5.4 [**37**, **38**]. We adopt the supercell model for PVK/C_{60} nanoheterojunction. The supercell is aligned along the z-axis. The vacuum layer in the simulation cell was set to 15 Å thick in both x- and y-directions to ensure negligible interactions between the supercell and its periodic images. The PVK/C_{60} nanoheterojunction was simulated using periodic boundary conditions. We have performed calculations using both the LDA in the Perdew-Zunger parametrization [**39**] and the GGA in the "Perdew-Burke-Ernzerhof parametrization [**40**]. We used the ultrasoft pseudopotentials [**41**] in describing the interactions between the ions and electrons. The plane wave basis sets method and the Perdew–Burke–Ernzerhof (PBE) exchange-correlation functional [**42**] were used to describe the exchange-correlation effects. In this work, the Grimme's D3 correction term [**43**] was applied to include the van der Waals (vdW) interaction which was found to be substantial in carbon nano systems [**44**-**46**]. For all the calculations, the plane-wave kinetic energy cutoff was set to 30 Ryd and charge density cut-off set to 180 Ryd. The energy convergence was set to be 0.002 Ryd, and all the configurations were fully relaxed until the residual force on each atom was less than 0.001 Ryd/Bohr. For all these DFT calculations, a Γ-centered 5x5x1 Monkhorst-Pack scheme [**47**] k-point grid was used to sample the Brillouin zone during the geometry optimization. Fine 9x9x1 grids for non-self-consistent field calculations was used in the computation to determine quantized energy levels and Fermi energy for band structure calculations along the Γ-Z-direction, density of electronic states (DOS) and partial density of electronic states (PDOS). Throughout this work, the figures related to the optimized configurations were generated using VESTA software [**48**]. The modelled supercells are visualized using the Xcrysden software, version 1.5.60 [**49**](49).

3. Results and Discussions

3.1 Structural properties of the Nanoheterostructures

Figure **1** depicts the nanoheterostructures investigated in this work. The following three configurations were studied: (a) the five-membered ring of C_{60} and the π-conjugate plane of PVK

were arranged in parallel configuration, (b) the six-membered ring of C_{60} and the π-conjugate plane of PVK were modelled in parallel arrangement, (c) in the third configuration, the six-membered ring of C_{60} was aligned to face the nitrogen containing ring of PVK nanostructure.

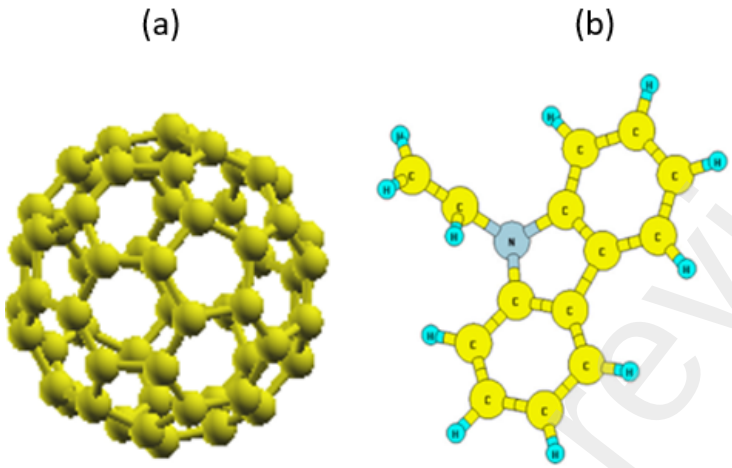

Figure **1**. Schematic illustration of PVK and C_{60} nanostructures.

The structural stability of the PVK/C_{60} nanoheterojunctions studied were evaluated by calculating both the adsorption energies and the formation energy per atom for each of the three described configurations to determine the most energetically favourable stacking nanoheterostructure using equations (1) and (2) below [**50**].

A separation distance of ~3.383Å was kept between PVK and C_{60} for all the three nanoheterojunctions designed. The interlayer distance calculated is comparable to the interlayer separations in graphite (ca. 3.35 Å). Relative to this adsorption distance of 3.383 Å, we calculated the adsorption energies, E_{ad}, for the PVK/C_{60} nanoheterojunctions as tabulated in Table 1. The adsorption energies, E_{ad}, were determined from the relation:

$$E_{ad} = \left(E_{PVK/C_{60}} - E_{PVK} - E_{C_{60}}\right) \quad (1)$$

where $E_{PVK/C_{60}}$, E_{PVK}, $E_{C_{60}}$ represent the total ground-state energy of the PVK/C_{60} composite, the total energy of PVK, the total energy of C_{60} respectively predicted by DFT calculation. Quantum Espresso code reports the value of dispersion contribution to total energy for every step during the geometry optimization process. Accordingly, the dispersion contribution to adsorption energy was determined using Equation 1 above, by replacing the terms on the right-hand side with the dispersion contribution quantities for the converged geometry of each structure.

Table 1. Adsorption Energy Determined Using Equation 1.

Model type (GGA+vdW)	Adsorption Energy (eV)
PVK/C_{60}(**a**)	1.239
PVK/C_{60}(**b**)	1.418
PVK/C_{60}(**c**)	2.236
Model type (LDA)	
PVK/C_{60}(**a**)	1.223
PVK/C_{60}(**b**)	1.335
PVK/C_{60}(**c**)	2.129

If the $E_{ad} > 0$, then it suggests that the surface adsorption is thermodynamically feasible. The greater the E_{ad} value, the tendency of the adsorbate molecule to bind on the PVK/C_{60} nanoheterostructure surface becomes stronger. From Table 1, a clear distinctive trend in the preferences of PVK/C_{60}(**a**), PVK/C_{60}(**b**) and PVK/C_{60}(**c**) nanoheterojunctions to adsorb favorably on PVK/C_{60} surface is seen.

From DFT optimized configurations of all the three systems we considered in this work, we found the interactions of PVK/C_{60}(**a**) and PVK/C_{60}(**b**) nanoheterojunctions are considerably weak compared to PVK/C_{60}(**c**), Table 1. Compared to the other configuration, the adsorption energies of PVK/C_{60}(**a**) and PVK/C_{60}(**b**) nanoheterojunctions are generally found to be the weakest, i.e., $E_a \sim 1.239, 1.418$ eV, for GGA+vdW exchange-correlation functional and $E_a \sim 1.223, 1.335$ eV for LDA exchange-correlation functional. These can be considered as physisorption processes on the surfaces. For PVK/C_{60}(**c**) nanoheterojunction, the adsorption energy, $E_a \sim 2.236, 2.129$ eV, for the respective exchange-correlation functionals, is attributed to the orientation and proximity of the nitride functional group of the polymer to the conjugated π-electrons of the fullerene(C_{60}) to chemisorb at the PVK/C_{60} surface. For the PVK/C_{60}(**c**) nanoheterojunction, the strongest tendency to chemisorb on the PVK/C_{60} surface is found, i.e., $E_a \sim 2.236$ eV, via strong π-π interactions between the carbazole unit and the fullerene(C_{60}).

The formation energies tabulated in Table 2 were determined from the relation:

$$\Delta E = E_{CHN} - N_C E_C - N_H E_H - N_N E_N \quad (2)$$

where E_{CHN} is the total energy of the ground state of the corresponding nanoheterojunction modelled. E_C is the total energy of carbon in its ground state (graphite), N_C is the number of carbon atoms in the nanoheterojunction. E_H is the total energy of ground state of H, N_H is the number of hydrogen atoms, E_N is the total energy of ground state of N and N_N is the number of nitrogen atoms in the nanoheterojunction modelled.

The calculated formation energies per atom for each of the nanoheterojunctions is tabulated in Table 2. It is observed that all of the new nanoheterojunctions modelled have negative formation energies per atom; an indication that these new structures are thermodynamically stable.

To gain further insight into the new structures, we calculated the formation energy per atom for C_{60} and the formation energy per atom for PVK separately and found their values to be − 5.263 eV and − 6.486 eV respectively which are much larger than all the formation energies per atom in Table 2 for each of the newly designed nanoheterojunctions in this present study. This shows that

the new nanoheterojunctions are more stable and thermodynamically favourable in comparison to the original molecules.

Table 2. Formation Energy Per Atom Calculated Using Equation 2.

Model type (GGA+vdW)	**Formation Energy (eV)**
PVK/C_{60}(**a**)	-6.183
PVK/C_{60}(**b**)	-8.224
PVK/C_{60}(**c**)	-10.681
Model type (LDA)	
PVK/C_{60}(**a**)	-5.991
PVK/C_{60}(**b**)	-7.295
PVK/C_{60}(**c**)	-10.169

Furthermore, our calculations reveal that in the nanoheterojunction model in which the six-membered ring of C_{60} faces the nitrogen containing ring of PVK, PVK/$C_{60}(c)$, is the most favoured and the most stable in both GGA+vdW and LDA model types as compared to PVK/$C_{60}(a)$ and PVK/$C_{60}(b)$ nanoheterojunctions.
As a result of the stacking patterns in the PVK/$C_{60}(a)$, PVK/$C_{60}(b)$ and PVK/$C_{60}(c)$ configurations, the three structures were found to shrink accordingly as shown in table 3. The values of the energy differences E_0(eV) of the simulated nanoheterojunctions show a progressive stability from stable to most stable nanoheterojunction respectively.

Table 3. Optimized Lattice Parameters a(Å), b(Å), c(Å), Energy gap Eg(eV) and Energy Difference E_0(eV) of PVK/C_{60}(**a**), PVK/C_{60}(**b**) and PVK/C_{60}(**c**) nanoheterojunctions.

(GGA+vdW)	**a(Å)**	**b(Å)**	**c(Å)**	**Eg(eV)**	**E_0(eV)**
PVK/C_{60}(**a**)	9.3283	9.3496	9.4579	1.223	17.362
PVK/C_{60}(**b**)	9.2770	8.5050	9.2936	1.217	9.212
PVK/C_{60}(**c**)	9.1311	10.1133	9.0673	1.121	0.000
Model type (LDA)					
PVK/C_{60}(**a**)	9.3019	8.6619	8.6958	1.218	15.379
PVK/C_{60}(**b**)	8.8500	7.0067	8.8528	1.201	7.804
PVK/C_{60}(**c**)	9.1350	10.3534	9.1376	1.112	0.000

In all the three nanoheterojunctions designed, observation reveals C−C bonds exhibit slightly smaller lengths in PVK/$C_{60}(a)$, PVK/$C_{60}(b)$ and PVK/$C_{60}(c)$ designs with 1.3928 Å, 1.3943 Å and 1.3934 Å respectively in GGA+vdW model type as compared to the experimental value of 1.42

Å. The C−N bond length for PVK/C_{60}(c) in LDA model type is 1.3918 Å as compared with PVK/C_{60}(a) and PVK/C_{60}(b) with 1.4126 Å and 1.4324 Å respectively, table 4.

Table 4. Optimized **C−N**, **C–C** & **C–H** Bond Lengths(**Å**) of PVK/C_{60} Nanoheterostructure.

Model type (GGA+vdW)	**Bond Length (Å)**		
	C−N	C – C	C – H
PVK/C_{60}(a)	1.4064	1.3928	1.0848
PVK/C_{60}(b)	1.4082	1.3943	1.0858
PVK/C_{60}(c)	1.4031	1.3934	1.0863
Model type (LDA)			
PVK/C_{60}(a)	1.4126	1.4198	1.0711
PVK/C_{60}(b)	1.4324	1.4211	1.0910
PVK/C_{60}(c)	1.3918	1.4169	1.0881

This indicates stronger intra-chain interactions in these nanoheterojunctions. In fact, shorter bond lengths and consequently stronger bonds are found to be indicative of more stability of the nanoheterojunctions. As a result, C−N bonds are found to be more stiffer in PVK/$C_{60}(c)$ and C–C bonds in PVK/$C_{60}(a)$ and PVK/$C_{60}(b)$ nanoheterojunctions which accounted for their stability and rigid nature. The changes observed in the bond lengths is as a result of the adsorption energies relative to the adsorption distance 3.383Å calculated above. The shorter C−C and C−N bonds in PVK/$C_{60}(a)$, PVK/$C_{60}(b)$ and PVK/$C_{60}(c)$ designs indicate that their covalent character has been strengthened compared with that before the adsorption. Thus, they tend to possess higher binding energies leading to much stronger bonding in these designs. Therefore, PVK/$C_{60}(a)$, PVK/$C_{60}(b)$ and PVK/$C_{60}(c)$ designs with shorter bond lengths and consequently stronger bonds strengths are expected to be indicative of more stability resulting in their rigidity due to a strong covalent bonding character.

From Table 2, it is observed that there are variations in the formation energy per atom calculated in accordance with the different choice of the exchange-correlation functionals. The values calculated with the LDA pseudopotentials are slightly lower as compared to the values calculated with the GGA pseudopotentials. The same trend is observed in the optimized lattice parameter values calculated in Table 3 with different exchange-correlation functionals LDA and GGA, with LDA giving almost smaller values of the lattice parameters. GGA+vdW calculations give the band-gap values for PVK/C_{60}(**a**), PVK/C_{60}(**b**) and PVK/C_{60}(**c**) nanoheterojunctions as 1.223, 1.217 and 1.121 eV respectively as against LDA calculations of 1.218, 1.201 and 1.112 eV respectively.

3.2 Electronic properties of the nanoheterojunctions

The electronic band structures at high-symmetry k-points for PVK/$C_{60}(a)$, PVK/$C_{60}(b)$ and PVK/$C_{60}(c)$ nanoheterojunctions are shown in Figure 2. The band gaps occur due to mixed

hybridization of valence states of N and H with that of C atoms in the respective nanoheterojunctions. The calculated band gap values along with the optimized lattice parameters and other structural values of all three model types are shown in Table 3.
Upon further analysis of the electronic band structure plots, Figures 2(a, b & c), it is observed that these nanoheterojunctions are narrow and direct band gap materials with the valance band and conduction band both located at the Γ-points. This then makes it a good candidate for photo physical applications because it is a preferred material for the fabrication of optoelectronic devices. These new materials have tunable band gaps and may find applications in various fields and are promising candidates to facilitate the development of band gap engineering for applications in photovoltaics and solar cells, infrared optoelectronics, nanoelectronics. By matching the band structures of C_{60} and PVK with the new modelled nanoheterojunctions it is revealed that the new bands are formed as a result of the hybridization of valence states in the new proposed nanoheterojunctions.

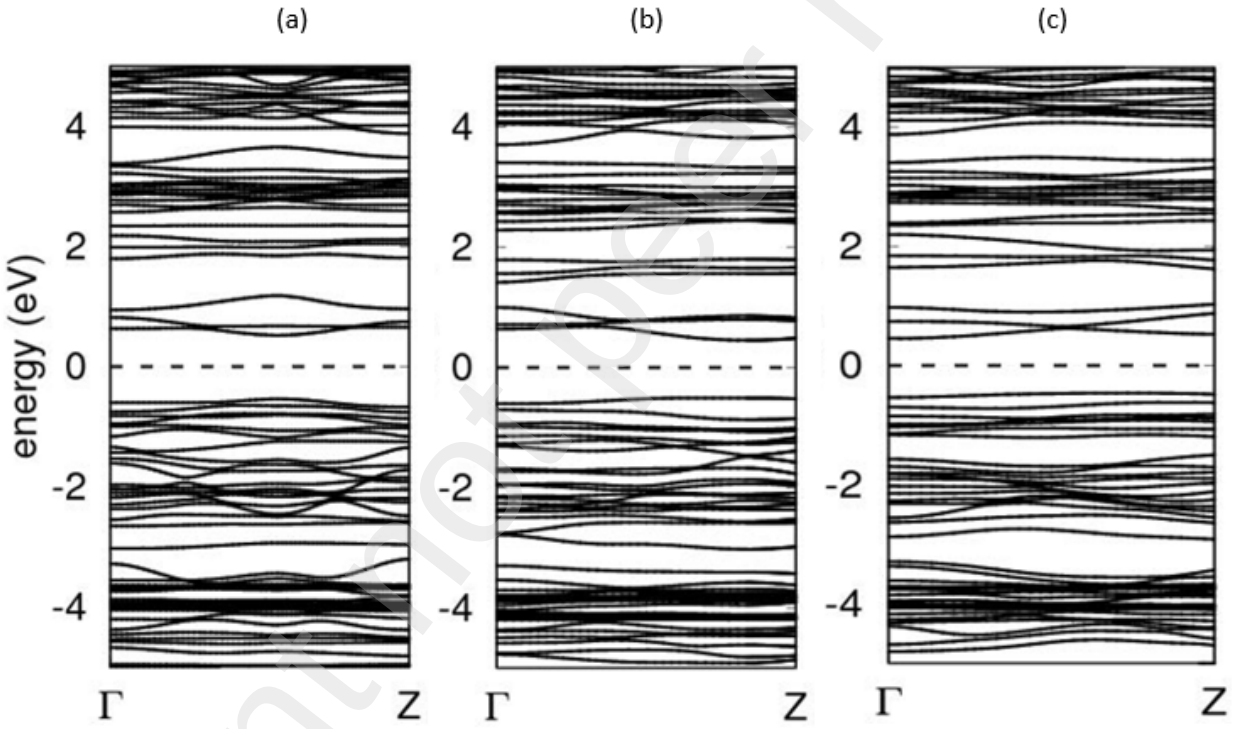

Figure **2**. Calculated band structures at high-symmetry k-points of the PVK/C_{60} nanoheterojunctions with fermi energy level set at zero for: (a) PVK/C_{60}(a), (b) PVK/C_{60}(b), (c) PVK/C_{60}(c) nanoheterojunctions respectively.

3.4 Analysis of the electronic density of states.

We further analyzed the nature of interactions and origin of energy gaps in these nanoheterojunctions by way of plotting the projected electronic DOS, total DOS (t-DOS) and partial DOS (p-DOS) of the individual PVK/C_{60} nanoheterojunctions in Figures 3, 4 and 5

respectively. For comparison, the Fermi energy, E_F, level was set as zero on the energy scale of the energy band-gap, Eg, between the occupied atomic orbitals and the empty atomic bands and the same for the DOS, which is shown in Figures 3, 4 and 5. The total and partial electron density of states (t-DOS and p-DOS) plainly reveal that, the portion of DOS below -4 eV is due to N and C atoms even though larger proportion of the contributions is coming from N atoms only. The central portion which is above -4 eV is due to the contributions from N and C atoms in addition to the contribution of H atoms. The Figures 3 and 4 show only positive contributions to the total and partial density of states of electrons for the PVK/C_{60} nanoheterojunctions.

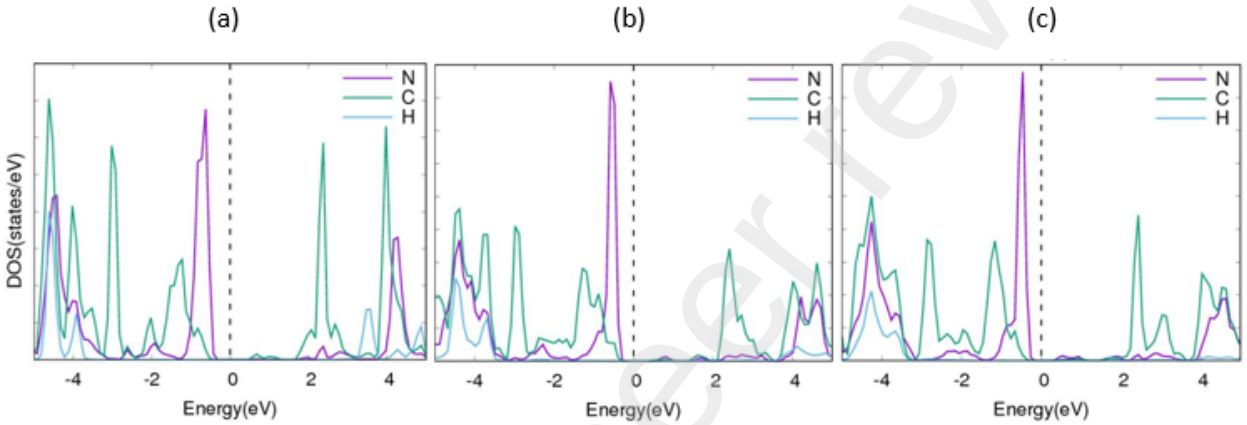

Figure **3**. Projected electronic density of states (DOS) for the PVK/C_{60} configuration with fermi energy level set at zero for: (a) PVK/$C_{60}(a)$, (b) PVK/$C_{60}(b)$, (c) PVK/$C_{60}(c)$ nanoheterojunctions respectively.

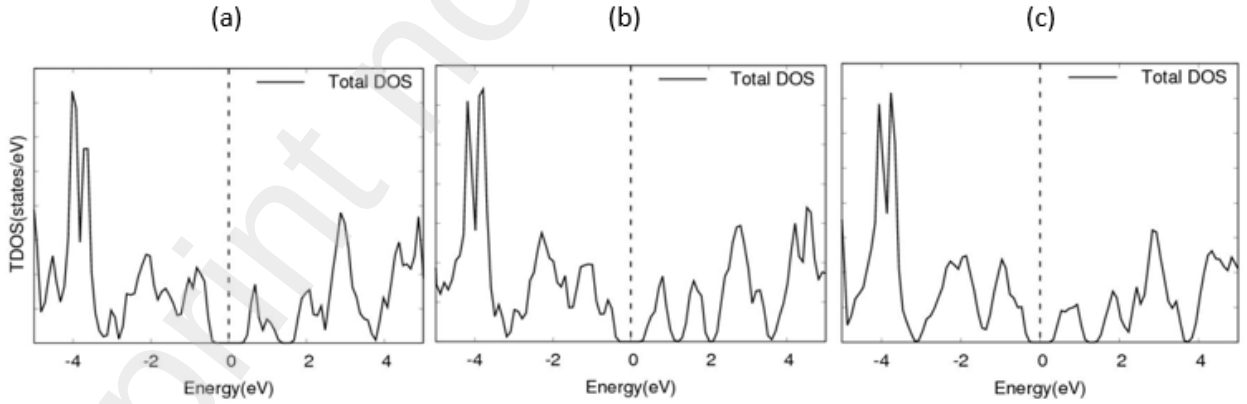

Figure **4**. Total electronic density of states (t-DOS) for the PVK/C_{60} configuration with fermi energy level set at zero for (a) PVK/$C_{60}(a)$, (b) PVK/$C_{60}(b)$, (c) PVK/$C_{60}(c)$ nanoheterojunctions respectively.

Upon the visualization of the atomic orbitals, we note that the DOS near the energy gaps is essentially of p_z electronic character manifestations of the anti-bonding and bonding of N atoms hybridizing with those of p_z states of carbon atoms. From the p-DOS shown in Figure 5, it can be seen that, the s- and p-orbitals of carbon and also p-orbitals of nitrogen are the dominant class of contributors to the valence bands and conduction band, i. e, both top of fully filled bands and the bottom of unoccupied bands are influenced by s- and p-orbital states of carbon and nitrogen atoms resulting in the non-covalent π-stacking in PVK/C_{60} nanoheterojunction configuration stackings as seen in Figures 1(a, b & c).

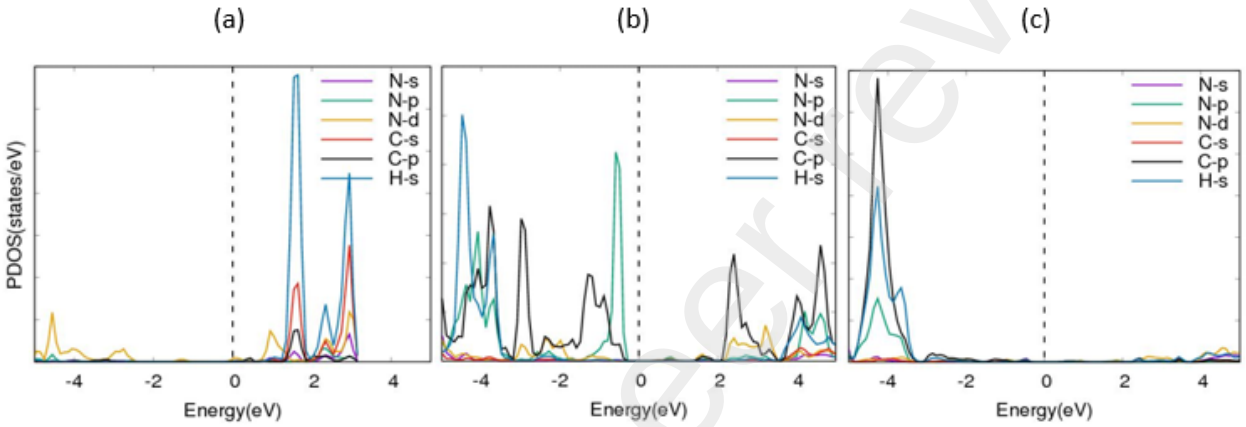

Figure **5**. Partial density of states (p-DOS) for the PVK/C_{60} configuration with fermi energy level set at zero for (a) PVK/$C_{60}(a)$, (b) PVK/$C_{60}(b)$, (c) PVK/$C_{60}(c)$ nanoheterojunctions respectively.

3.5 Optical properties

3.5.1 Optical Absorption Spectra

Figures 6(a – e) show calculated optical spectral absorption for (a) PVK, (b) C_{60}, (c) PVK/C_{60}(a), (d) PVK/C_{60}(b) and (e) PVK/C_{60}(c) nanostructures respectively. Figures 6(a, b) show the absorption spectra for pristine PVK and C_{60}. Figures 6(c – e) are the calculated absorption spectra for the nanoheterojunctions when the C_{60} was added. In Figure 6(a), it can be observed that there are five intensity peaks located at 0.41, 0.45, 0.49, 0.51 and 0.53 Ry. The most intense peak is located at 0.41 Ry. In Figure 6(b), we observed that there are distinctive absorption levels for each direction. Comparing Figure 6(b) with Figure 6(c), it is observed that on addition of the C_{60} absorption in the Y-direction exceeds absorption in the Z-direction. Also from Figure 6(b), it is observed that absorptions in X-, Y- and Z- directions are almost the same with that of Y- slightly above them. From Figure (e), X- direction has the least absorption with the absorption in the Y-direction exceeding absorption in the Z- direction.

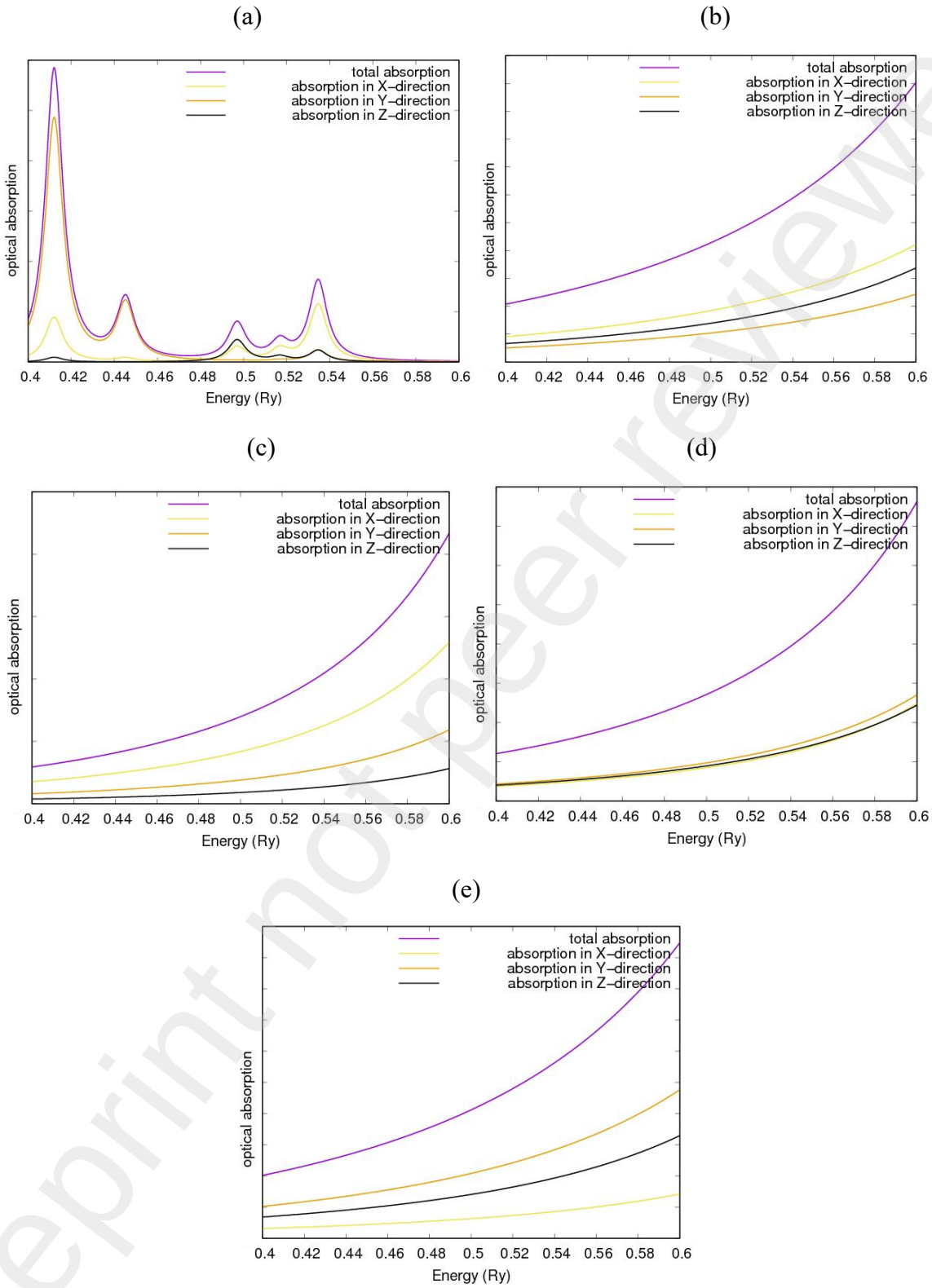

Figure **6**.: Calculated optical absorption spectra for (a) PVK, (b) C_{60}, (c) PVK/C_{60}(a), (d) PVK/C_{60}(b), (e) PVK/C_{60}(c) nanostructures respectively.

These observations are indications of charge transfer processes occurring between the C_{60} and PVK. The C_{60} incorporation within the polymer network affects the PVK ring deformation and stretching. This means that there is a direct interaction between the C_{60} and the main PVK chain through charge transfer processes.

3.6 Lowdin Charge Transfer

The amount of charge transfer from PVK to the C_{60} was estimated by projecting the charge density onto the atomic orbitals. We calculated the charge transfer as the difference between the Lowdin charges for pristine PVK and PVK/C_{60} with the adsorbate molecules. From this result, we determined whether the adsorbate molecule acts as an acceptor or as a donor. The charge transfer from the polymer, PVK, to the fullerene, C_{60}, in the configuration of PVK/$C_{60}(c)$ turns out to be 0.19 electrons respectively, whereas for the configurations PVK/$C_{60}(a)$ and PVK/$C_{60}(b)$ we computed 0.11 and 0.12 electrons respectively in the opposite direction. Here we would like to point out that it is important to note that the size of the charge transfer slightly depends on the method chosen for calculations.

Conclusion

To obtain the structural and electronic properties of the effects of different orientations of stacking structures of PVK/C_{60} nanoheterojunctions, we performed systematic structural search to identify low energy configurations of various polymer/fullerene nanoheterojunctions. Our calculations give a reliable understanding of the role of intermolecular interactions between PVK and C_{60} and the effect of incorporation of C_{60} on electronic and optical properties of PVK. The DFT-based optimization of PVK/C_{60} nanoheterojunctions produce lattice parameters and bond lengths accurate to within a few percent of the experimental values depending on choice of exchange-correlation functional. The C_{60} incorporation within the polymer network affects the PVK ring deformation and stretching. This means that there is a direct interaction between the C_{60} and the main PVK chain through charge transfer processes. The PVK/C_{60} nanoheterojunctions exhibit extreme characteristics of vdW materials and are expected to be p-type semiconductors with suitable band gaps, high electron mobility for applications in optoelectronics, sensors, thermoelectric devices and possibly mid-infrared photodetectors. We propose a PVK/C_{60} nanoheterojunction as a potential candidate for use in nanoelectronics devices. Finally, we emphasize that the present approach is generally applicable for the analysis for solar cells and photovoltaics, including the exciton transfers, charge transports, as well as the multistate dynamics from the exciton to free carriers.

Acknowledgments

The authors would like to acknowledge the financial support from the Ghana Government Book and Research Allowance for tertiary institutions. V. W. E. acknowledges financial support from the University of Ghana Pan African Doctoral Academy (PADA) and also thanks the Ministry of Science and Technology for the grant of FICCI of New Delhi for fellowship. Authors are grateful

to the Centre for High Performance Computing (CHPC), Cape Town, South Africa, for computer time on the Lengau" cluster.

Funding

This research received no external funding.

Conflict of interest Disclosure

The author(s) declare(s) that there is no conflict of interest regarding the publication of this paper.

Data Availability Statement

The DFT data used to support the findings of this study are included within the article.

References

[1] Http://www.konarka.com/.
[2] M. P. Anantram, F. Léonard, Rep. Prog. Phys. 69 (2006) 507–561.
[3] J. Laranjeira, L. Marques, M. Melle-Franco, K. Strutynski, M. Mezouar, M. Barroso. Materials Letters X, 4 (2019) 100026 https://doi.org/10.1016/j.mlblux.2019.100026.
[4] M.S. Dresselhaus, G. Dresselhaus, P.C. Eklund, Science of Fullerenes and Carbon Nanotubes, Academic Press, 1996, ISBN 0-12-221820.
[5] A. Hirsch, M. Brettreich, Fullerenes: Chemistry and reactions, Wiley, 2005, ISBN 3-527-30820-2.
[6] D. M. Guldi, Acc. Chem. Res. 33 (2000) 695–703.
[7] L. Echengoyen, L. E. Echengoyen, Acc. Chem. Res. 31 (1998) 593–601.
[8] Universita` di Milano Bicocca.
[9] D. Dini, M. J. F. Calvete, M. Hanack, Chem. Rev. 116 (2016) 13043–13233.
[10] P. G. Lacroix, I. Malfant, C. Lepetit, Coord. Chem. Rev. 308 (2016) 381–394.
[11] W. Chen, Z. R. Li, D. Wu, Y. Li, C. C. Sun, F. L. Gu, J. Am. Chem. Soc. 127 (2005) 10977–10981.
[12] G. de la Torre, P. Vaquez, F. Agullo-Lopez, T. Torres, Chem. Rev. 104 (2004) 3723–3750.
[13] S. Jeon, J. Haley, J. Flikkema, V. Nalla, M. Wang, M. Sfeir, L. S. Tan, T. Cooper, W. Ji, M. R. Hamblin, L. Y. Chiang, J. Phys. Chem. C117 (2013) 17186–17195.
[14] P. Aloukos, K. Iliopoulos, S. Couris, D. M. Guldi, C. Sooambar, A. Mateo-Alonso, P. G. Nagaswaran, D. Bonifazi, M. Prato, J. Mater. Chem. 21 (2011) 2524–2534.
[15] N. Tang, J. P. Partanen, R. W. Hellwarth, R. J. Knize, Phys. Rev. B48 (1993) 8404–8408.
[16] L. W. Tutt, A. Kost, Nature 356 (1992) 225–226.
[17] P. M. Ajayan, O. Stephan, C. Colliex, D. Trauth, Sci. 265 (1994) 1212–1214.
[18] R. H. Baughman, A. A. Zakhidov, W. A. Heer, Sci. 197 (2002) 787–92.
[19] V. W. Elloh, V. A. Apalangya, G. H. Gebreyesus, K. M. Abhishek, K. Kan Dapaah, E. Nyankson, J. K. Efavi, B. Onwona-Agyeman, A. Yaya, A theoretical study of the structural and electronic properties of poly (9-vinylcarbazole) interacting with small diameter single-

walled carbon nanotubes, Int. Jour. of Compu. Mat. Sci. & Eng. 9 (2020) 2050009. DOI: 10.1142/S2047684120500098.
[20] L. Dai, Polym. Adv. Tech. 10 (1999) 357–420.
[21] G. Z. Chen, M. S. P. Shaffer, D. Coleby, G. Dioxan, W. Zhou, D. J. Fray, Adv. Mater. 12 (2000) 522–526.
[22] Y. Saito, S. Uemura, K. Hamaguchi, Jpn. J. Appl. Phys. 37 (1998) L346–8.
[23] S. A. Curran, P. M. Ajayan, W. J. Blau, D. L. Carroll, J. N. Coleman, A. B. Dalton, Adv. Mater. 10 (1998) 1091–3.
[24] V. W. Elloh, E. K. K. Abavare, K. M. Abhishek, G. H. Gebreyesus, A. Yaya, Computational Modelling of Structural, Electronic, Optical and Vibrational Properties of PVK/C_{60} Nanoheterostructure Interfaces, Jour. of Bioint. Res. in Appl. Chem. 11 (2020) 10864-10884. DOI: 10.33263/BRIAC113.1086410884.
[25] H. Ago, K. Petritch, M. S. P. Shaffer, A. H. Windle, R. H. Friend, Adv. Mat. 11 (1999) 1281–5.
[26] R. D. Pensack, J. B. Asbury, J. Phys. Chem. Lett. 1 (2010) 2255–2263.
[27] H. Imahori, N. V. Tkachenko, V. Vehmanen, K.Tamaki, H. Lemmetyinen, Y. Sakata, S. Fukuzumi, J. Phys. Chem. A105 (2001) 1750–1756.
[28] R. A. Marcus, Rev. Mod. Phys. 65 (1993) 599–610.
[29] J. G. S. Ramon, E. R. Bittner, J. Phys. Chem. B110 (2006) 21001–21009.
[30] E. R. Bittner, J. G. S. Ramon, S. Karabunarliev, J. Chem. Phys. 122 (2005) 214719.
[31] H. Tamura, J. G. S. Ramon, E. R. Bittner, I. Burghardt, Phys. Rev. Lett. 100 (2008) 107402.
[32] H. Tamura, J. G. S. Ramon, E. R. Bittner, I. Burghardt, J. Phys. Chem. B112 (2008) 495–506.
[33] H. Tamura, E. R. Bittner, I. Burghardt, J. Chem. Phys. 127 (2007) 034706.
[34] V. W. Elloh, K. M. Abhishek, D. Dodoo-Arhin, E. K. K. Abavare, G. H. Gebreyesus, E. Nyankson, J. K. Efavi, B. Onwona-Agyeman, A. Yaya, Structural and Electronic properties of PVK/C60 Nanoheterostructure interfaces – A DFT Approach, Jour. of Surf. and Inter. 20 (2020) 100556.
[35] H. Tamura, E. R. Bittner, I. Burghardt, J. Chem. Phys. 126 (2007) 021103.
[36] H. Tamura, Coherent. J. Chem. Phys. 130 (2009) 214705–18.
[37] P. Giannozzi, O. Andreussi, T. Brumme, O. Bunau, M. Buongiorno Nardelli, Advanced capabilities for materials modelling with Quantum ESPRESSO, J. Phys. Conde. Matt. 2017, 29.
[38] http://www.quantum-espresso.org.
[39] J. P. Perdew, A. Zunger, Phys. Rev. B23 (1981) 5048–5079.
[40] J. P. Perdew, K. Burke, M. Ernzerhof, Phys. Rev. Lett. 77 (1996) 3865–3868.
[41] A. M. K. Rappe, M. Rabe, E. Kaxiras, J. D. Joannopoulos, Optimized pseudopotentials Phys. Rev. B 41 (1990) 1227–1230, doi.org/10.1103/PhysRevB.41.1227.
[42] J. P. Perdew, K. Burke, M. Ernzerhof, Generalized Gradient Approximation Made Simple. Phys. Rev. Lett. 77 (1996) 3865.
[43] S. Grimme, J. Antony, S. Ehrlich, H. Krieg, A Consistent and Accurate Ab Initio Parametrization of Density Functional Dispersion Correction (DFT-D) for the 94 Elements H-Pu. J. Chem. Phys. 132 (2010) 154104.
[44] H. Park, H. S. Koh, D. J. Siegel, First-Principles Study of Redox End Members in Lithium–Sulfur Batteries. J. Phys. Chem. C119 (2015) 4675–4683.

[45] Q. Guo, K. C. Lau, R. Pandey, A Xanes Study of Lithium Polysulfide Solids: A First-Principles Study. Mater. Adv. 2 (2021) 6403–6410.
[46] Q. Guo, K. C. Lau, R. Pandey, Thermodynamic and Mechanical Stability of Crystalline Phases of Li_2S_2, J. Phys. Chem. C 123 (2019) 4674–4681.
[47] Q. Sun, K. C. Lau, D. Geng, X. Meng, Atomic and Molecular Layer Deposition for Superior Lithium-Sulfur Batteries: Strategies, Performance, and Mechanisms. Batter. Super. 1 (2018) 41–68.
[48] K. Momma, F. Izumi, Vesta 3 for Three-Dimensional Visualization of Crystal, Volumetric and Morphology Data. J. Appl. Crystal. 44 (2011) 1272–1276.
[49] A. Kokalj, Computer graphics and graphical user interfaces as tools in simulations of matter at the atomic scale. Comp. Mater. Sci. 28 (2003) 155-168.
[50] X. L. Hu, Y. F. Zhang, N. F. Zhuang, J. Q. Qian, Journal of Sol.-Stat. Chem. 183 (2010) 2741.